Theoretical Surface Science

Wintersemester 2007/08

Axel Groß

Universität Ulm, D-89069 Ulm, Germany
http://www.uni-ulm.de/theochem

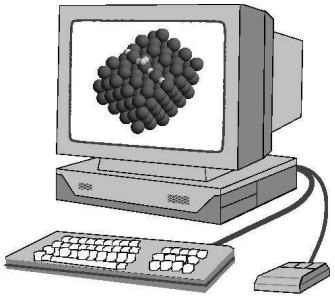

Outline

1. Introduction

Surfaces

- Processes on surfaces play an enormously important technological role
- Harmful processes:
  1. Rust, corrosion
  2. Wear
- Advantageous processes:
  1. Production of chemicals
  2. Conversion of hazardous waste

Theoretical approach

- Some decades ago: phenomenological thermodynamic approach prevalent
- Nowadays: microscopic approach
- Theoretical surface science no longer limited to explanatory purposes
- Many surface processes can indeed be described from first pricinples, i.e., without invoking any empirical parameter

Here: microscopic perspective of theoretical surface science

Experiment: a wealth of microscopic information available:
STM, REMPI, QLEED, HREELS, . . .

Surface and image potential states

Cu(111) DFT surface band structure

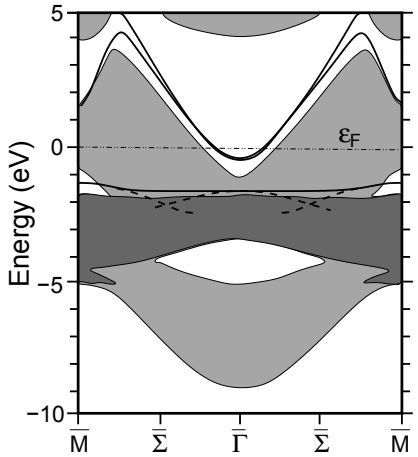

Cu(111): Band gas and parabolic surface band at the $\bar{\Gamma}$-Point

A. Euceda, D.M. Bylander, and L. Kleinman, Phys. Rev. B **28**, 528 (1983)

Cu(100): Image potential states

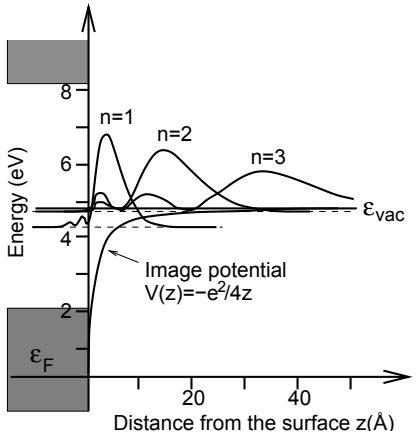

Rydberg image potential states observable with time-resolved photo electron spectroscopy

U. Höfer, I.L. Shumay, Ch. Reuß, U. Thomann, W. Wallauer, and Th. Fauster, Science **277**, 1480 (1997)

Cu(111) surface states

Don Eigler, IBM Almaden

Quantum Corral

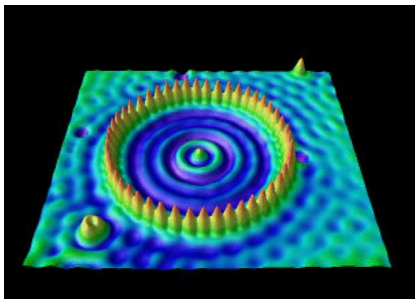

48 Fe atoms on Cu(111) placed in a circle with diameter 71 Å

M.F. Crommie *et al.*, Science **262**, 218 (1993).

Quantum Mirage

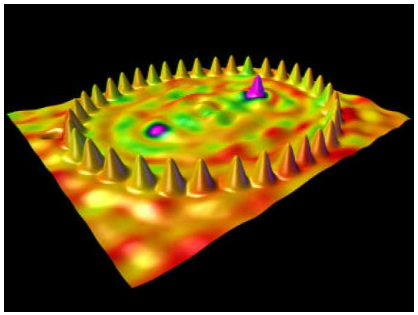

Elliptival *Quantum Corral* with a Co atom at the focus of the ellipse

H.C. Manoharan *et al.*, Nature **403**, 512 (2000).

Diffusion on surfaces: oxygen atoms on Ru(0001)

STM images

Oxygen diffusion

Diffusion barriers of oxygen on Ru(0001) rather high so that there are only few jumps to adjacent sites at room temperature.

50 consecutive images of
oxygen atoms on Ru(0001)
at room temperature on 13% coverage
Scan rate: 8 images per second

Joost Wintterlin et.al., FHI Berlin
http://w3.rz-berlin.mpg.de/pc/stm/WS-fstm.html

Non-linear phenomenon on surfaces

Theoretical Modelling

Photo- emission electronmicroscopy-(PEEM) image of a Pt(110) surface at 4×10^{-4} mbar O_2 and 4.3×10^{-5} mbar CO partial pressures at a temperature of $T = 448$ K (A. Nettesheim *et al.*, JCP **98**, 9977 (1993)).

Reaction scheme for the description of CO oxidation on Pt(110)

$$\mathrm{CO} + * \leftrightarrow \mathrm{CO}^{(\mathrm{ads})}\,, \quad (1)$$

$$\mathrm{O_2} + * \rightarrow 2\mathrm{O}^{(\mathrm{ads})}\,, \quad (2)$$

$$\mathrm{O}^{(\mathrm{ads})} + \mathrm{CO}^{(\mathrm{ads})} \rightarrow 2* + \mathrm{CO_2}\,, \quad (3)$$

$$1\times2 \leftrightarrow 1\times1\ . \quad (4)$$

Kinetik: $u = \theta_{\mathrm{CO}},\ v = \theta_{\mathrm{O}},\ w = \theta_{1\times1}$

$$\dot{u} = s_{\mathrm{CO}}\, p_{\mathrm{CO}} - k_2 u - k_3 uv + D\nabla^2 u, \quad (5)$$

$$\dot{v} = s_{\mathrm{O_2}}\, p_{\mathrm{O_2}} - k_3 uv, \quad (6)$$

$$\dot{w} = k_5\,[f(u) - w], \quad (7)$$

Manipulation of reaction fronts by laser

J. Wolff, A.G. Papathanasiou, I.F. Kevrekidis, H.H. Rotermund, G. Ertl, Science **294**, 134 (2001)

Reaction fronts locally manipulated by heating through a laser spot (diameter 80 μm).

H.H. Rotermund et.al., FHI Berlin
http://w3.rz-berlin.mpg.de/ rotermun/science/index.html

Hydrogen dimer vacancy on hydrogen-covered Pd(111)

Salmeron *et al.*, Nature **422**, 705 (2003); PRL **93**, 146103 (2004).

Dimer vacancies appear as triangles because of the rapid diffusion of the hydrogen atoms at the rim
No adsorption events into dimer vacancy found

Adsorption of H_2/(3×3)7H/Pd(100)

Ab initio MD simulation of H_2/Pd(100) for a kinetic energy of 100 meV

Dissociation

Trapping

Significant energy transfer to pre-adsorbed hydrogen atoms upon the dissociative adsorption

Dissociation dynamics of H_2/(6×6)Pd(100)

Ab initio MD simulation of H_2/(6×6)Pd(100) for a kinetic energy of 200 meV

Trajectories

Animation

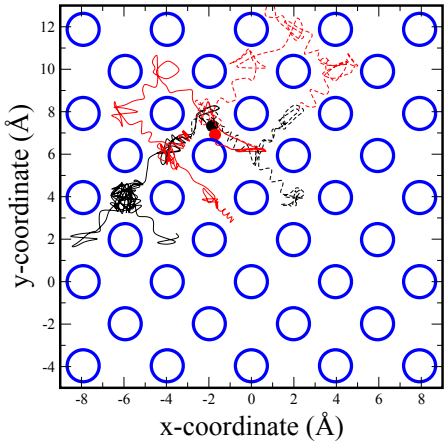

Atoms can stay relatively close to each other

Molecular adsorption: O_2/Pt(111)

$E_{\rm kin} = 1.1$ eV

Energy redistribution

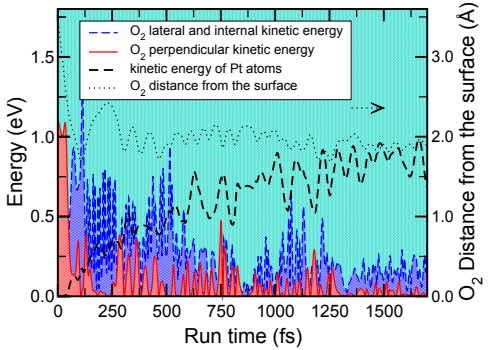

Calculated TBMD trajectory with an initial kinetic energy of $E_{\rm kin} = 0.2$ eV

Energy redistribution during the run time of the trajectory

Energy transfer of the impinging molecule into lateral and internal degrees of freedom ⇒ Trapping into a dynamical precursor state

KMC simulation of the growth of Al(111)

Simulation (1/8 of simulation area = 600×600 array)

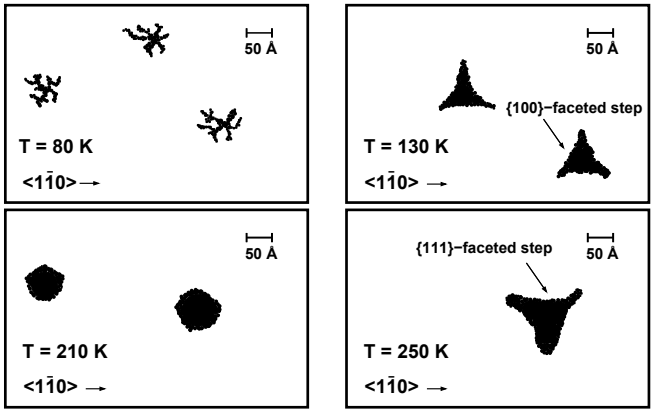

Deposition flux 0.08 ML/s, coverage $\theta = 0.08$ ML

P. Ruggerone *et al.*, Prog. Surf. Sci. **54**, 331 (1997)

Growth of a compound semiconductor: GaAs

31 processes (barriers) explicitly considered by DFT as an input for KMC simulations, prefactor: $10^{13}\mathrm{s}^{-1}$

P. Kratzer and M. Scheffler, Phys. Rev. Lett. **88**, 036102 (2002).

Front view

Top view

2. Hamiltonian

Solid-state physics and chemistry:
Only electrostatic interaction considered ⇒ Hamiltonian:

$$H = T_{\mathrm{nucl}} + T_{\mathrm{el}} + V_{\mathrm{nucl-nucl}} + V_{\mathrm{nucl-el}} + V_{\mathrm{el-el}} \tag{8}$$

$$T_{\mathrm{nucl}} = \sum_{\mathrm{I}=1}^{L} \frac{\vec{P}_{\mathrm{I}}^{2}}{2M_{\mathrm{I}}}, \tag{9}$$

$$T_{\mathrm{el}} = \sum_{\mathrm{i}=1}^{N} \frac{\vec{p}_{\mathrm{i}}^{2}}{2m}, \tag{10}$$

$$V_{\mathrm{nucl-nucl}} = \frac{1}{2} \sum_{\mathrm{I} \neq \mathrm{J}} \frac{Z_{\mathrm{I}}\, Z_{\mathrm{J}}\, e^2}{|\vec{R}_{\mathrm{I}} - \vec{R}_{\mathrm{J}}|}, \tag{11}$$

$$V_{\mathrm{nucl-el}} = -\sum_{\mathrm{i,I}} \frac{Z_{\mathrm{I}}\, e^2}{|\vec{r}_{\mathrm{i}} - \vec{R}_{\mathrm{I}}|}, \tag{12}$$

$$V_{\mathrm{el-el}} = \frac{1}{2} \sum_{\mathrm{i} \neq \mathrm{j}} \frac{e^2}{|\vec{r}_{\mathrm{i}} - \vec{r}_{\mathrm{j}}|}. \tag{13}$$

Magnetic effects could be explicitly included

Schrödinger equation

Nonrelativistic Schrödinger equation:

$$H\ \Phi(\vec{R}, \vec{r}) = E\ \Phi(\vec{R}, \vec{r}). \tag{14}$$

In principle we are ready here, however

solution of Schrödinger equation in closed form not possible

⇒ **Hierarchy of approximations**

Born-Oppenheimer approximation

Atoms 10^4 to 10^5 heavier than electrons
(except for hydrogen and helium)
⇒electrons are 10^2 to 10^3 times faster than the nuclei

Born-Oppenheimer of adiabatic approximation:
electrons follow motion of the nuclei instantaneously

Practical implementation:
Define electronic Hamiltonian H_{el} for fixed nuclear coordinates $\{\vec{R}\}$

$$H_{\mathrm{el}}(\{\vec{R}\}) = T_{\mathrm{el}} + V_{\mathrm{nucl-nucl}} + V_{\mathrm{nucl-el}} + V_{\mathrm{el-el}}. \tag{15}$$

Nuclear coordinates $\{\vec{R}\}$ do not act as variables but as parameters
The Schrödinger equation for the electrons

$$H_{\mathrm{el}}(\{\vec{R}\})\ \Psi(\vec{r}, \{\vec{R}\}) = E_{\mathrm{el}}(\{\vec{R}\})\ \Psi(\vec{r}, \{\vec{R}\}). \tag{16}$$

Born-Oppenheimer approximation II

Schrödinger equation for the electrons

$$H_{\rm el}(\{\vec{R}\})\ \Psi(\vec{r},\{\vec{R}\}) \ = \ E_{\rm el}(\{\vec{R}\})\ \Psi(\vec{r},\{\vec{R}\}). \tag{17}$$

$E_{\rm el}(\{\vec{R}\})$ Born-Oppenheimer energy surface: potential for the nuclear motion:

$$\{T_{\rm nucl} + \ E_{\rm el}(\vec{R})\}\ \chi(\vec{R}) \ = \ E_{nucl}\ \chi(\vec{R}). \tag{18}$$

If quantum effects negligible: classical equation of motion

$$M_{\rm I}\ \frac{\partial^2}{\partial t^2}\vec{R}_I \ = \ -\frac{\partial}{\partial \vec{R}_I}E_{\rm el}(\{\vec{R}\}) \quad . \tag{19}$$

Forces evaluated according to the Hellmann-Feynman theorem

$$\mathbf{F}_{\rm I} \ = \ -\frac{\partial}{\partial \vec{R}_{\rm I}}E_{\rm el}(\{\vec{R}\}) \ = \ \langle\Psi(\vec{r},\{\vec{R}\})|\frac{\partial}{\partial \vec{R}_{\rm I}}H_{\rm el}(\{\vec{R}\})|\Psi(\vec{r},\{\vec{R}\})\rangle \tag{20}$$

Born-Oppenheimer approximation (BOA) III

In the BOA electronic transitions neglected

Exact derivation: Expansion of Schrödinger equation in the small parameter m/M

BOA very successful, but still its validity hardly directly obvious

Physical arguments

Systems with a band gap: electronic transitions improbable

Metals: electronic system strongly coupled
$\Rightarrow$ short lifetimes and fast quenchening of electronic excitations

Structure of the Hamiltonian in Surface Science

Interaction of a system with few degrees of freedom, atoms or molecules, with a system, the surface or substrate, that has in principle infinitely many degrees of freedom.

quantum chemistry $\leftrightarrow$ solid-state methods.

Symmetries

- First step: Determine symmetries of the Hamiltonian
- $\Rightarrow$ Group theory
- Provides exact results
- Reduces computationally cost dramatically

Exploitation of symmetries

T operator of a symmetry transformation
$\Rightarrow$ H and T commute, i.e. $[H,T]=0$.

$\Rightarrow \langle\psi_i|H|\psi_j\rangle = 0,$
if $|\psi_i\rangle$ and $|\psi_j\rangle$ are eigenfunctions of T belonging to different eigenvalues $T_i \neq T_j$.

$\Rightarrow$ Only functions with the same symmetry couple in the Hamiltonian

Three-dimensional periodic systems

3D crystal lattice

Bravais lattice:

$$\vec{R} \ = \ n_1\vec{a}_1 \ + \ n_2\vec{a}_2 \ + \ n_3\vec{a}_3. \tag{21}$$

$\mathbf{a}_i$ linearly independent unit vectors, n_i integer

14 Bravais lattices in three dimensions

Dual space to real space: Reciprocal space

$$\vec{b}_1 \ = \ 2\pi\ \frac{\vec{a}_2\times\vec{a}_3}{|\vec{a}_1(\vec{a}_2\times\vec{a}_3)|} \tag{22}$$

$\vec{b}_2$ and $\vec{b}_3$: cyclic permutation of the indices

$$\vec{a}_{\rm i}\ \cdot\ \vec{b}_{\rm j} \ = \ 2\pi\ \delta_{\rm ij}, \tag{23}$$

Miller indices

Lattice planes described by the shortest reciprocal lattice vector $h\vec{b}_1 + k\vec{b}_2 + h\vec{b}_3$ perpendicular to this plane

Integer coefficients hkl: Miller indices.

Lattice planes: (hkl)

Family of lattice planes: $\{hkl\}$

Directions: $[hkl]$

Face-centered cubic (fcc) and body-centered cubic (bcc) crystals:
Miller indices are usually related to the underlying simple cubic lattice

Bloch Theorem

Bloch theorem illustrates power of group theory

Hamiltonian

Consider effective one-particle Schrödinger equation

$$\left\{-\frac{\hbar^2}{2m}\nabla^2 + v_{eff}(\vec{r})\right\}\psi_i(\vec{r}) = \varepsilon_i\psi_i(\vec{r}). \quad (24)$$

Effective one-particle potential $v_{eff}(\vec{r})$ satisfies translational symmetry:

$$v_{eff}(\vec{r}) \;=\; v_{eff}(\vec{r}\,+\,\vec{R}), \quad (25)$$

with $\vec{R}$ any Bravais lattice vector.

Exploitation of group theory

Translations $T_{\vec{R}}$ form an Abelian group
$\Rightarrow$ 1-D representation, eigenfunctions:

$$T_{\vec{R}}\psi_i(\vec{r}) = \psi_i(\vec{r}+\vec{R}) = c_i(\vec{R})\psi_i(\vec{r}) \quad (26)$$

$$\text{with} \quad c_i(\vec{R})c_i(\vec{R}') = c_i(\vec{R}+\vec{R}'). \quad (27)$$

$$\Rightarrow c_i(\vec{R}) \;=\; e^{i\vec{k}\cdot\vec{R}}. \quad (28)$$

Eigenfunction $\psi_i(\vec{r})$ characterized by the *crystal-momentum* $\vec{k}$

$$\psi_{\vec{k}}(\vec{r}) \;=\; e^{i\vec{k}\cdot\vec{r}}\,u_{\vec{k}}(\vec{r}) \quad (29)$$

with the periodic function

$$u_{\vec{k}}(\vec{r}) \;=\; u_{\vec{k}}(\vec{r}\,+\,\vec{R}) \quad (30)$$

Structure of Surfaces

Surface: created by just cleaving an infinite crystal along one surface plane.

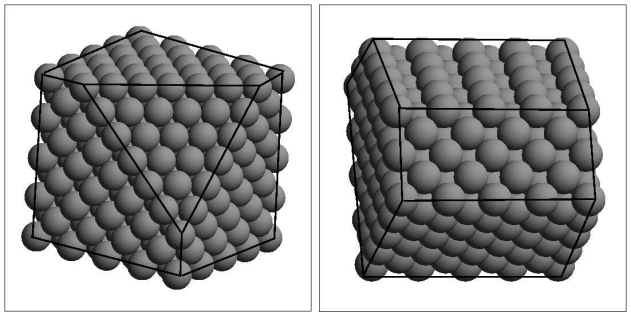

Left panel: fcc crystal with 100 faces and one 111 face,
right panel: fcc crystal with 100 faces and one 110 face.

Bravais Lattices in 2 Dimensions

2D lattice	sketch	examples
Square $\lvert\vec{a}_1\rvert = \lvert\vec{a}_2\rvert$ $\varphi = 90°$	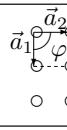	fcc(100) 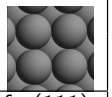
Hexagonal $\lvert\vec{a}_1\rvert = \lvert\vec{a}_2\rvert$ $\varphi = 120°$	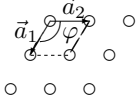	fcc(111) 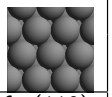
Rectangular $\lvert\vec{a}_1\rvert \neq \lvert\vec{a}_2\rvert$ $\varphi = 90°$		fcc(110) 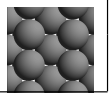

2D lattice	sketch	examples
Centered rectangular $\lvert\vec{a}_1\rvert \neq \lvert\vec{a}_2\rvert$ $\varphi = 90°$	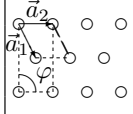	bcc(110) 
Oblique $\lvert\vec{a}_1\rvert \neq \lvert\vec{a}_2\rvert$ $\varphi \neq 90°$	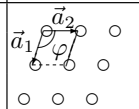	fcc(210) 

Ideal, Relaxed and Reconstructed (110) Surfaces

Structure	Ideal	Relaxed	Reconstructed
	1×1	1×1	2×1
Top view			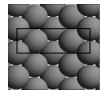
Side view			

Changed surface periodicity:

unit cell spanned by
$\mathbf{a}_1^s = m\mathbf{a}_1$ and $\mathbf{a}_2^s = n\mathbf{a}_2$:

surface labelled by $(hkl)(m \times n)$
or $(hkl)p(m \times n)$, p primitive

centered structures:
$(hkl)c(m \times n)$

Ideal surface: interatomic distances the same as in the bulk
Relaxed surface: rearrangement preserving surface symmetry
Reconstructed surface: symmetry of surface changed

Vicinal Surfaces

Vicinal surface: A surface that is only slightly misaligned from a low index plane

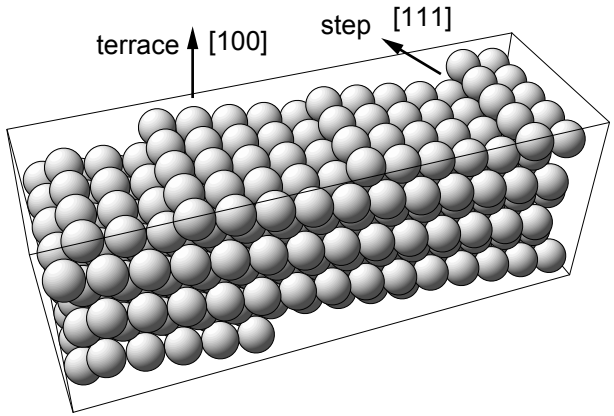

A stepped $(911) = 5(100) \times (111)$ vicinal surface.

Vicinal surfaces also denoted by $n(hkl) \times (h'k'l')$,
(hkl) and $(h'k'l')$ Miller indices of the terraces and of the ledges,
n width of the terraces in number of atomic rows parallel to the ledges.

Defects at Surfaces

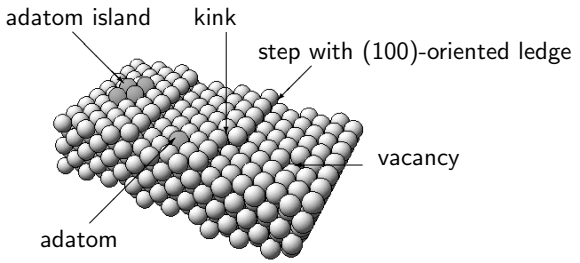

Defected $(755) = 5(111) \times (100)$ surface

Study of defects important:

steps, kinks and other surface irregularities often dominate surface processes such as surface reactions, oxidation, corrosion, crystal growth or surface melting.

Electronic Structure methods

Time-independent electronic Schrödinger equation

$$H_{\rm el}\ \Psi(\vec{r}) \ = \ E_{\rm el}\ \Psi(\vec{r}). \tag{31}$$

Parametric dependence on the nuclear coordinates omitted

Mathematically Schrödinger equation corresponds to a partial differential equation in $3N$ unknows with N commonly larger than 100 $\Rightarrow$ completely intractable to solve

Way out:

expand the electronic wave function in some suitable, but necessarily finite basis set

$\Rightarrow$ Conversion of the partial differential equation into a set of algebraic equations that are much easier to handle.

Quantum mechanical approach for the electronic structure problem

Rayleigh-Ritz variational principle

Ground state energy E_0,
$|\Psi\rangle$ arbitrary guess for the true ground state wave function $|\Psi_0\rangle$:

$$E_0 \ \leq \ \frac{\langle\Psi|H|\Psi\rangle}{\langle\Psi|\Psi\rangle}. \tag{32}$$

Rayleigh-Ritz variational principle

provides a route to come closer to the true ground state energy by improving the guesses for $|\Psi\rangle$, preferentially in a systematic way.

Independent electrons

Assumption: N electrons in the effective external potential

$$v_{ext}(\vec{r}) \ = \ -\sum_{\rm I} \frac{Z_{\rm I}\ e^2}{|\vec{r} - \vec{R}_{\rm I}|} \tag{33}$$

$\Rightarrow$ One-particle Schrödinger equation

$$\left\{ -\frac{\hbar^2}{2m}\nabla^2 \ + \ v_{ext}(\vec{r}) \right\} \psi_i(\vec{r}) \ = \ \varepsilon_i^o\, \psi_i(\vec{r}). \tag{34}$$

$\Rightarrow$ Product wave function solution for many-body wave function

$$\Psi_{\rm H}(\vec{r}_1, \ldots, \vec{r}_{\rm N}) \ = \ \psi_1(\vec{r}_1) \cdot \ldots \cdot \psi_{\rm N}(\vec{r}_{\rm N}) \tag{35}$$

Hartree Approximation I

Assume product wave function as a first guess for the many-body wave function

$\Rightarrow$ Expection value of the electronic Hamiltonian:

$$\langle\Psi_{\rm H}|H|\Psi_{\rm H}\rangle = \sum_{i=1}^{N}\int d\vec{r}\;\psi_i^*(\vec{r})\;\left(-\frac{\hbar^2}{2m}\nabla^2 \;+\; v_{ext}(\vec{r})\right)\psi_i(\vec{r})$$
$$+\frac{1}{2}\sum_{i,j=1}^{N}\int d\vec{r}d\vec{r}'\;\frac{e^2}{|\vec{r}-\vec{r}'|}\;|\psi_i(\vec{r})|^2|\psi_j(\vec{r}')|^2 + V_{\rm nucl-nucl}. \qquad (36)$$

Minimize the expectation value (36) with respect to more suitable single-particle functions $\psi_i(\vec{r})$ under the constraint that the wave functions are normalized:

$$\frac{\delta}{\delta\psi_k^*}\left[\langle\Psi_{\rm H}|H|\Psi_{\rm H}\rangle \;-\; \sum_{i=1}^{N}\{\varepsilon_i(\langle\psi_i|\psi_i\rangle \;-\; 1)\}\right] \;=\; 0. \qquad (37)$$

ε_i: Lagrange multipliers ensuring the normalisation of the eigen functions.

Hartree Approximation II

Variation leads to the *Hartree equations*

$$\left\{-\frac{\hbar^2}{2m}\nabla^2 \;+\; v_{ext}(\vec{r}) \;+\; \sum_{j=1}^{N}\int d\vec{r}'\;\frac{e^2}{|\vec{r}-\vec{r}'|}\,|\psi_j(\vec{r}')|^2\right\}\psi_k(\vec{r}) \;=\; \varepsilon_k\,\psi_k(\vec{r}). \qquad (38)$$

Mean-field approximation: Hartree equations describe an electron embedded in the electrostatic field of *all electrons including the particular electron itself*.
This causes the *self interaction* which is erroneously contained in the Hartree equations.

Define electron density $n(\vec{r})$ and *Hartree potential* $v_{\rm H}$:

$$n(\vec{r}) \;=\; \sum_{i=1}^{N}|\psi_i(\vec{r})|^2, \qquad v_{\rm H}(\vec{r}) \;=\; \int d\vec{r}'\;n(\vec{r}')\;\frac{e^2}{|\vec{r}-\vec{r}'|} \qquad (39)$$

$\Rightarrow$ Hartree equations:

$$\left\{-\frac{\hbar^2}{2m}\nabla^2 \;+\; v_{ext}(\vec{r}) \;+\; v_{\rm H}(\vec{r})\right\}\psi_i(\vec{r}) \;=\; \varepsilon_i\;\psi_i(\vec{r}). \qquad (40)$$

Hartree Approximation III

Hartree equations:

$$\left\{-\frac{\hbar^2}{2m}\nabla^2 \;+\; v_{ext}(\vec{r}) \;+\; v_{\rm H}(\vec{r})\right\}\psi_i(\vec{r}) \;=\; \varepsilon_i\;\psi_i(\vec{r}). \qquad (41)$$

Solutions $\psi_i(\vec{r})$ of the Hartree equations enter the effective one-particle Hamiltonan:

$\Rightarrow$ Hartree equations can only be solved in an iterative fashion

$\Rightarrow$ Hartree approximation $\equiv$ "self-consistent field approximation".

Expectation value of the total energy in the Hartree approximation $E_{\rm H}$:

$$\begin{aligned}\langle\Psi_{\rm H}|H|\Psi_{\rm H}\rangle \;&=\; \sum_{i=1}^{N}\varepsilon_i \;-\frac{1}{2}\int d\vec{r}\;d\vec{r}'\;\frac{e^2\;n(\vec{r})\;n(\vec{r}')}{|\vec{r}-\vec{r}'|} \;+V_{\rm nucl-nucl}\\ &=\; \sum_{i=1}^{N}\varepsilon_i \;-\; V_{\rm H} \;+\; V_{\rm nucl-nucl} \;=\; E_{\rm H}\end{aligned} \qquad (42)$$

Hartree energy $V_{\rm H}$ enters the Hartree eigenvalues twice $\Rightarrow$ has to be subtracted.
Reflects the interaction between particles in a self-consistent scheme.

Self-consistent field solution

Effective one-particle Hartree-Fock Hamiltonians contain solution:
$\Rightarrow$ Self-consistent iteration scheme

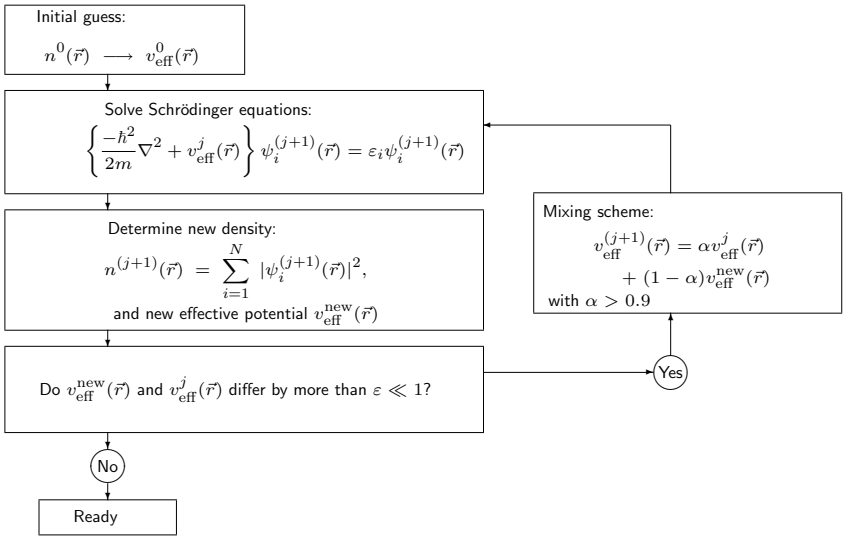

Flow-chart diagram of a self-consistent field solution scheme

Hartree-Fock Approximation I

Hartree ansatz only partially obeys the Pauli principle
by populating each electronic state once,

but it does not take into account the anti-symmetry of the wave function.

$\Rightarrow$ Construction of a Slater determinant from the single-particle functions $\psi(\vec{r}\sigma)$, where σ denotes the spin:

$$\Psi_{\rm HF}(\vec{r}_1\sigma_1,\ldots,\vec{r}_{\rm N}\sigma_{\rm N}) \;=\; \frac{1}{\sqrt{N!}} \begin{vmatrix} \psi_1(\vec{r}_1\sigma_1) & \psi_1(\vec{r}_2\sigma_2) & \ldots & \psi_1(\vec{r}_{\rm N}\sigma_{\rm N}) \\ \psi_2(\vec{r}_1\sigma_1) & \psi_2(\vec{r}_2\sigma_2) & \ldots & \psi_2(\vec{r}_{\rm N}\sigma_{\rm N}) \\ \vdots & \vdots & \ddots & \vdots \\ \psi_{\rm N}(\vec{r}_1\sigma_1) & \psi_{\rm N}(\vec{r}_2\sigma_2) & \ldots & \psi_{\rm N}(\vec{r}_{\rm N}\sigma_{\rm N}) \end{vmatrix} . \qquad (43)$$

Hartree-Fock Approximation II

Follow same procedure as in the Hartree ansatz: first write down expectation value

$$\begin{aligned} \langle\Psi_{\rm HF}|H|\Psi_{\rm HF}\rangle \;=\; & \sum_{i=1}^{N} \int d\vec{r}\; \psi_i^*(\vec{r}) \left(-\frac{\hbar^2}{2m}\nabla^2 \;+\; v_{ext}(\vec{r}) \right) \psi_i(\vec{r}) \\ & + \frac{1}{2} \sum_{i,j=1}^{N} \int d\vec{r}\; d\vec{r}\,' \; \frac{e^2}{|\vec{r}-\vec{r}\,'|} \; |\psi_i(\vec{r})|^2 \; |\psi_j(\vec{r}\,')|^2 \\ & - \frac{1}{2} \sum_{i,j=1}^{N} \int d\vec{r} d\vec{r}\,' \frac{e^2}{|\vec{r}-\vec{r}\,'|} \; \delta_{\sigma_{\rm i}\sigma_{\rm j}} \psi_i^*(\vec{r})\psi_i(\vec{r}\,')\psi_j^*(\vec{r}\,')\psi_j(\vec{r}). \\ & + V_{\rm nucl-nucl} \; . \end{aligned} \qquad (44)$$

$\sigma_{\rm i}$ spin of the state $\psi_i(\vec{r})$

Hartree-Fock Approximation III

Minimize expectation value of total energy with respect to the ψ_i^* under the constraint of normalization:

$$\begin{aligned} & \left\{ -\frac{\hbar^2}{2m}\nabla^2 \;+\; v_{ext}(\vec{r}) \;+\; v_{\rm H}(\vec{r}) \right\} \psi_i(\vec{r}) \\ & \quad - \sum_{j=1}^{N} \int d\vec{r}\,' \; \frac{e^2}{|\vec{r}-\vec{r}\,'|} \; \psi_j^*(\vec{r}\,')\psi_i(\vec{r}\,')\psi_j(\vec{r})\delta_{\sigma_{\rm i}\sigma_{\rm j}} \;=\; \varepsilon_i \; \psi_i(\vec{r}). \end{aligned} \qquad (45)$$

Additional term, *exchange term*, integral operator: $\int V(\vec{r},\vec{r}\,')\psi(\vec{r}\,')d\vec{r}\,'$

Total energy in the Hartree-Fock approximation:

$$\langle\Psi_{\rm HF}|H|\Psi_{\rm HF}\rangle \;=\; E_{\rm HF} \;=\; \sum_{i=1}^{N} \varepsilon_i \;-\; V_{\rm H} \;-\; E_{\rm x} \;+\; V_{\rm nucl-nucl} \qquad (46)$$

Homogeneous electron gas

Homogeneous electron gas: $n(\vec{r})$ uniform.

Assumption: electrostatic potential of the electrons
compensated by a positive charge background.

$\Rightarrow$ "jellium model":

$$v_{ext}(\vec{r}) \;+\; v_{\rm H}(\vec{r}) = 0 \; . \qquad (47)$$

Eigenfunctions of the Hartree equations for the homogeneous electron gas
(periodic boundary conditions):

$$\psi_{\rm i}(\vec{r}) \;=\; \frac{1}{\sqrt{V}} \; e^{i\vec{k}_{\rm i}\cdot\vec{r}}. \qquad (48)$$

Plane waves

Exchange in the homogeneous electron gas

Total energy: Hartree term $V_{\rm H}$ exactly cancels with $V_{\rm nucl-nucl}$

$$E_{\rm H} \;=\; \sum_{i=1}^{N} \varepsilon(\vec{k}_{\rm i}) \;=\; 2 \sum_{|\vec{k}|<k_{\rm F}} \frac{\hbar^2 \vec{k}^2}{2m}. \tag{49}$$

Fermi vector $k_{\rm F}$: vector of the occupied one-electron levels of highest energy,

$$k_{\rm F} \;=\; \left(3\pi^2 \frac{N}{V}\right)^{1/3} \;=\; \left(3\pi^2 n\right)^{1/3} \tag{50}$$

Hartree-Fock: plane waves are still eigenfunctions for the homogeneous electron gas

$$\varepsilon(\vec{k}) \;=\; \frac{\hbar^2 \vec{k}^2}{2m} \;-\; \frac{2e^2}{\pi}\, k_{\rm F}\, F\left(\frac{k}{k_{\rm F}}\right) \tag{51}$$

$$F(x) \;=\; \frac{1}{2} \;+\; \frac{1-x^2}{4x}\, \ln\left|\frac{1+x}{1-x}\right|. \tag{52}$$

One-particle energies

One-particle energies for the homogeneous electron gas in the Hartree and the Hartree-Fock approximation:

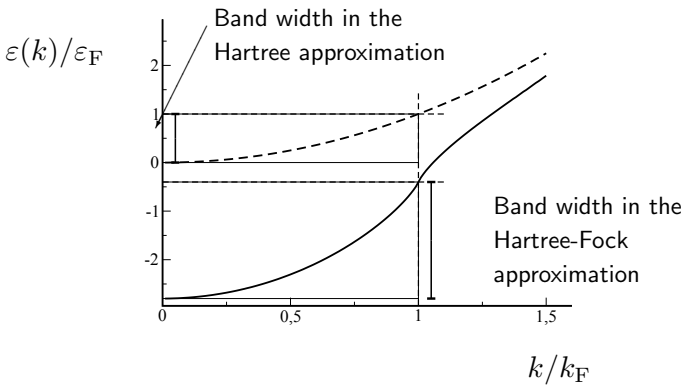

Total energy in the Hartree-Fock approximation

Total energy for the homogeneous electron gas:

$$\begin{aligned} E_{\rm HF} \;&=\; 2 \sum_{k<k_{\rm F}} \frac{\hbar^2 \vec{k}^2}{2m} \;-\; \sum_{k<k_{\rm F}} \frac{e^2}{\pi}\, k_{\rm F}\, F\left(\frac{k}{k_{\rm F}}\right) \\ &=\; N\left(\frac{3}{5}\,\varepsilon_{\rm F} \;-\; \frac{3}{4}\,\frac{e^2}{\pi}\, k_{\rm F}\right). \end{aligned} \tag{53}$$

Exchange energy $\varepsilon_{\rm x}$ per electron in the homogeneous electron gas

$$\begin{aligned} \varepsilon_{\rm x} \;&=\; -\frac{3}{4}\,\frac{e^2}{\pi}\left(3\pi^2 n\right)^{1/3} \\ &=\; -\frac{3}{4}\,\frac{e^2}{\pi}\left(\frac{9\pi}{4}\right)^{1/3} \frac{1}{r_s} \end{aligned} \tag{54}$$

with the Wigner-Seitz radius $r_s \;=\; \left(\dfrac{3}{4\pi n}\right)^{1/3}$, (55)

Exchange hole distribution

Exchange-hole density $n_x^i(\vec{r},\vec{r}')$ around the i-th electron:

$$n_x^i(\vec{r},\vec{r}') \;=\; -\sum_{j=1}^{N} \frac{\psi_j^*(\vec{r}')\psi_i(\vec{r}')\psi_j(\vec{r})}{\psi_i(\vec{r})}\, \delta_{\sigma_{\rm i}\sigma_{\rm j}}\,. \tag{56}$$

The exchange-hole density satisfies

$$\int d\vec{r}'\; n_x^j(\vec{r},\vec{r}') \;=\; -1 \tag{57}$$

$\Rightarrow$ Exchange term in the Hartree-Fock equations

$$\begin{aligned} -\sum_{j=1}^{N} \int d\vec{r}'\, \frac{e^2}{|\vec{r}-\vec{r}'|}\, \psi_j^*(\vec{r}')\psi_i(\vec{r}')\psi_j(\vec{r})\delta_{\sigma_{\rm i}\sigma_{\rm j}} \\ =\; \int d\vec{r}'\, \frac{e^2}{|\vec{r}-\vec{r}'|}\, n_x^j(\vec{r},\vec{r}')\psi_i(\vec{r}) \end{aligned} \tag{58}$$

Exchange hole in the homogeneous electron gas

Mean exchange-hole density in the homogeneous electron gas:

$$n_x(\vec{r},\vec{r}') = \sum_{i=1}^{N} \frac{\psi_i^*(\vec{r}')n_x^i(\vec{r},\vec{r}')\psi_i(\vec{r})}{n(\vec{r}')}\,\delta_{\sigma_i\sigma_j}\,; \quad |\vec{r}-\vec{r}'| = \bar{r}$$

$$= n_x(\bar{r}) = \frac{9}{2}\frac{N}{V}\left(\frac{k_F\bar{r}\cos(k_F\bar{r}) - \sin(k_F\bar{r})}{(k_F\bar{r})^3}\right)^2 . \qquad (59)$$

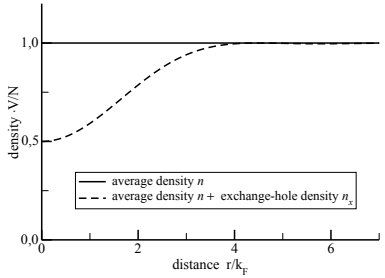

Electron correlation

Hartree-Fock: electrons of same spin are correlated, but not electrons of opposite spin

Further reduction in energy, if electrons of opposite spin are also correlated

Exchange and exchange-correlation energy per particle in the homogeneous electron gas:

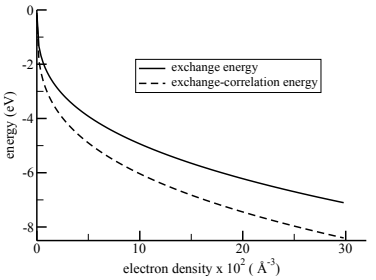

Typical valence electron densities of metals are in the range of 5 - 10 $\times$ 10^2 ($Å^{-3}$).

Quantum chemistry methods I

Cluster

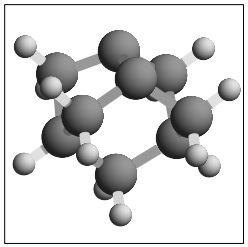

Si_9H_{12} cluster used to model a Si(100) substrate

Quantum chemistry

- Historically, chemists were the first to be interested in the theoretical description of surfaces and processes at surfaces
- Theoretical tools used by chemists are made to describe finite systems such as molecules
- $\Rightarrow$ In the chemistry approach surfaces are regarded as big molecules and modelled by finite clusters
- This ansatz is guided by the idea that bonding on surfaces is a local process. It depends on the localisation of the electronic orbitals.

Quantum chemistry methods II

Hartree-Fock

- Usually Hartree-Fock theory good starting point for a theoretical description: exact total energy of a molecule is often reproduced to up to 99%
- Unfortunately, the missing part, namely the electron correlation energy, is rather important for a reliable description of chemical bond formation.
- Correlation energy per electron can easily be more than 1 eV ($\rightarrow$ free electron gas)

Requirements

- 1 kcal/mol $\approx$ 0.04 eV ("chemical accuracy") for energy differences required
- Quantum chemists have developped a whole machinery of theoretical methods that treat the electron correlation at various levels of sophistication: MP2, CI, CISD, FCI, CCSD, CCSD(T), MCSCF, CASSCF, . . .
- Methods can be devided into to two categories: the so-called single-reference and the multiple-reference methods.

Single reference methods

Starting point: Slater determinant

Hartree-Fock: correlation between electrons of opposite spin neglected

Ansatz: introduce correlation effects by considering excited states.

Generate excited states by replacing occupied orbitals in the Slater determinant by unoccupied ones

By replacing one, two, three, four or more states, single, double, triple, quadruple or higher excitations can be created.

Møller-Plesset theory: excitations are treated perturbatively

Møller-Plesset theory (MP)

Regard the Hartree-Fock Hamiltonian as the unperturbed Hamiltonian and the difference H' to the true many-body Hamiltonian as the perturbation

$$H' = H_{\mathrm{el}} - H_{\mathrm{HF}}. \tag{60}$$

Second-order expression (MP2):

$$E^{(2)} = E_{\mathrm{HF}} + \langle \Psi_0 | H' | \Psi_0 \rangle + \sum_{l \neq 0} \frac{|\langle \Psi_l | H' | \Psi_0 \rangle|^2}{E_0 - E_l}. \tag{61}$$

Higher-order corrections: MP3, MP4, ...

MP2 rather popular, but due to the perturbative treatment of electron correlation its applicability is still limited

Configuration Interaction (CI)

Instead of perturbative treatment include excitations explicitly in the wave:

$$\Psi_{\mathrm{CISD}} = \Psi_{\mathrm{HF}} + \sum c_i^{(1)} \Psi_i^{(1)} + \sum c_i^{(2)} \Psi_i^{(2)}. \tag{62}$$

Optimum wave function found by varying the coefficients $c_i^{(j)}$

Different configurations (or Slater determinants) are included in (62)
$\Rightarrow$ method called *configuration interaction* (CI)

If only single (S) and double (D) excitations are included: CISD

If all possible excitations are included: Full CI (FCI)

Size consistency

CISD approach does not fulfil *size consistency* or *size extensivity*

Size extensitivity: linear scaling of the energy with the number of electrons

Infinitely separated systems: additive energies of the separated components

This property is not only important for large systems, but even for small molecules

Product of two fragment CISD wave functions contains triple and quadruple excitations and is therefore no CISD function

$\Rightarrow$ no size-consistency

Coupled Cluster Theory (CC)

Recover size extensitivity by exponentiating single and double excitations operator:

$$\Psi_{\mathrm{CCSD}} = \exp(T_1 + T_2)\, \Psi_{\mathrm{HF}}. \tag{63}$$

Coupled cluster (CC) theory

Limitation to single and double excitations: CCSD

Triple excitations included: CCSDT

CCSDT has an eight-power dependence on the size of the system

Perturbative treatment of triple excitations: CCSD(T)

CCSD(T) calculations are method of choice for very accurate determination of molecular equilibrium structures

Multiple reference methods

Single-reference methods very reliable in the vicinity of equilibrium configurations

Often they are not adequate to describe a bond-breaking process:

Dissociation products should be described by a linear combination of two Slater determinants taking into account the proper spin state

$\Rightarrow$ One Slater determinant plus excited states derived from this determinant not sufficient

Accuracy can be systematically improved by considering more and more configurations
$\Rightarrow$ Full configuration interaction (FCI)

Because of the large required computational effort, FCI calculations are limited to rather small systems.

Approximate multi-reference methods are needed

SCF methods

Multiconfigurational self-consistent field (MCSCF) approach:

A relatively small number of configurations selected and both the orbitals and the configuration interactions coefficients are determined variationally

$\Rightarrow$ Chemical insight needed for the selection of the configurations

Complete active space (CASSCF) approach:

A set of active orbitals identified and all excitations within this active space are included.

Method computationally very costly

Basis set nomenclature

Preferred basis set in quantum chemistry: Gaussian functions
$\Rightarrow$ integral can be evaluated analytically

Nomenclature:

One atomic orbital per valence state: "minimal basis set" or "single zeta"

Two or more orbitals: "double zeta" (DZ), "triple zeta" (TZ) and so on

Often polarization functions added (one or more sets of d functions on first row atoms): "P" added to the acronym of the basis, e.g., DZ2P

Delocalized states (anionic or Rydberg excited states): further diffuse functions added

Density functional theory (DFT)

Wave function based methods limited to a small number of atoms due to unfavorable scaling

Electronic structure methods based on density more efficient: DFT

DFT based upon the Hohenberg-Kohn theorem:

The ground-state density $n(\vec{r})$ of a system of interacting electrons in an external potential uniquely determines this potential

Proof simple!

Density $n(\vec{r})$ uniquely related to the external potential and the number N of electrons via $N = \int n(\vec{r}) d\vec{r}$

$\Rightarrow$ $n(\vec{r})$ determines the full Hamiltonian

In principle it determines all quantities that can be derived from the Hamiltonian such as, e.g., the electronic excitation spectrum

Unfortunately this has no practical consequences since the dependence is only implicit

Variational principle

Variational principle for the energy functional:

$$E_{\rm tot} \;=\; \min_{n(\vec{r})} E[n] \;=\; \min_{n(\vec{r})} (T[n] \;+\; V_{\rm ext}[n] \;+\; V_{\rm H}[n] \;+ E_{\rm xc}[n]). \tag{64}$$

$V_{\rm ext}[n]$ functional of the external potential
$U[n]$ functional of the classical electrostatic interaction energy (Hartree energy)
$T[n]$ is the kinetic energy functional for **non-interacting** electrons

All quantum mechanical many-body effects are contained in the so-called exchange-correlation functional $E^{\rm xc}[n]$
This non-local functional is not known in general

Important property: $E^{\rm xc}[n]$ universal functional of the electron density

Advantage: Instead of using the many-body quantum wave function which depends on $3N$ coordinates now only a function of three coordinates has to be varied.

Kohn-Sham equations

In practice no direct variation of the density is performed because, e.g., the kinetic energy functional $T[n]$ is not well-known

Express density as a sum over single-particle states

$$n(\vec{r}) \;=\; \sum_{i=1}^{N} |\psi_i(\vec{r})|^2, \tag{65}$$

Minimize $E[n]$ with respect to the single particle states under the constraint of normalization: $\Rightarrow$ Kohn-Sham equations

$$\left\{ -\frac{\hbar^2}{2m}\nabla^2 \;+\; v_{ext}(\vec{r}) \;+\; v_{\rm H}(\vec{r}) \;+\; v_{\rm xc}(\vec{r}) \right\} \psi_i(\vec{r}) \;=\; \varepsilon_i \; \psi_i(\vec{r}) \; . \tag{66}$$

Exchange-correlation potential $v_{\rm xc}(\vec{r})$:

$$v_{\rm xc}(\vec{r}) \;=\; \frac{\delta E_{\rm xc}[n]}{\delta n}. \tag{67}$$

Again: "single-particle energies" ε_i enter the formalism just as Lagrange multipliers.

Ground state energy in DFT

Ground state energy

$$E \;=\; \sum_{i=1}^{N} \varepsilon_i \;+\; E_{\rm xc}[n] \;-\; \int v_{\rm xc}(\vec{r}) n(\vec{r}) \; d\vec{r} - \; V_{\rm H} \tag{68}$$

If the exchange-correlation terms $E_{\rm xc}$ and $v_{\rm xc}$ are neglected $\Rightarrow$ Hartree approximation

Difference to Hartree and the Hartree-Fock approximation:

Ground-state energy (102) is in principle exact

Reliability of any practical implementation of DFT depends crucially on the accuracy of the expression for the exchange-correlation functional

Exchange-correlation functional

Exchange-correlation functional $E_{\rm xc}[n]$:

$$E_{\rm xc}[n] \;=\; \int d\vec{r}\; n(\vec{r})\; \varepsilon_{\rm xc}[n](\vec{r}), \tag{69}$$

Introduce exchange-correlation hole distribution

$$n_{\rm xc}(\vec{r},\vec{r}') \;=\; g(\vec{r},\vec{r}') \;-\; n(\vec{r}')\;, \tag{70}$$

$g(\vec{r},\vec{r}')$ conditional density to find an electron at $\vec{r}'$ if there is already an electron at $\vec{r}$

Sum rules:

$$\int d\vec{r}'\; n_{\rm xc}(\vec{r},\vec{r}') \;=\; -1 \tag{71}$$

$$n_{\rm xc}(\vec{r},\vec{r}') \underset{|\vec{r}-\vec{r}'|\to\infty}{\longrightarrow} 0\;. \tag{72}$$

$$\int d\vec{r}'\; \frac{n_{\rm xc}(\vec{r},\vec{r}')}{|\vec{r}-\vec{r}'|} \underset{|\vec{r}|\to\infty}{\longrightarrow} -\frac{1}{|\vec{r}|} \tag{73}$$

Local Density Approximation (LDA)

Exchange-correlation energy per particle $\varepsilon_{\rm xc}[n](\vec{r})$ not known in general

Local density approximation: use exchange-correlation energy for the homogeneous electron gas also for non-homogeneous situations

$$E_{\rm xc}^{\rm LDA}[n] \;=\; \int d^3\vec{r}\; n(\vec{r})\; \varepsilon_{\rm xc}^{\rm LDA}(n(\vec{r})) \tag{74}$$

In a wide range of bulk and surface problems LDA surprisingly successful

Reasons still not fully understood, probably:

Cancellation of opposing errors in the LDA exchange and correlation

LDA satisfies the sum rules

For chemical reactions in the gas phase and at surfaces, however, the LDA results are not sufficiently accurate.

Usually LDA shows *over-binding*, i.e. binding and cohesive energies are too large and lattice constants and bond lengths are too small

Generalized Gradient Approximation (GGA)

Straightforward Taylor expansion of the exchange-correlation energy $\varepsilon^{\rm xc}[n]$:

Sum rules violated

Generalized gradient approximation: modify dependence on the gradient in such a way as to satisfy sum rules

$$E_{\rm xc}^{\rm GGA}[n] \;=\; \int d^3\vec{r}\; n(\vec{r})\; \varepsilon_{\rm xc}^{\rm GGA}(n(\vec{r}),|\nabla n(\vec{r}|)\;, \tag{75}$$

DFT calculations in the GGA achieve chemical accuracy (error $\leq$ 0.1 eV) for many chemical reactions; Example:

Dissociation barrier for H_2/Cu(111)

LDA: 0.05 eV PW91-GGA: 0.6 eV Exp.: 0.5 - 0.7 eV

Problematic systems within the GGA

There are important systems where GGA functionals do not give satisfactory results:

O_2 binding energy for different exchange-correlation functionals:

(B. Hammer, L.B. Hansen, and J.K. Nørskov, Phys. Rev. B **59**, 7413 (1999))

functional	LDA	PW91	PBE	revPBE	RPBE	Exp.
Binding energy (eV)	7.30	6.06	5.99	5.63	5.59	5.23

Due to the error in O_2 binding energies, O_2 adsorption energies in dissociative adsorption will be unreliable, too.

General problem: non-locality of the exchange-correlation functional

approximation uncontrolled, i.e., there is no systematic way of improving the functionals since there is no expansion in some controllable parameter

Pseudopotential

Chemical properties of most atoms are determined by their valence electrons.
$\Rightarrow$ Pseudopotentials

Schrödinger equation with pseudopotential

$$\left\{ -\frac{\hbar^2}{2m}\nabla^2 \; + \; v_{\rm ps} \right\} \mid \psi_{\rm ps} \rangle \; = \; \varepsilon_v \mid \psi_{\rm ps} \rangle \; . \tag{76}$$

with

$$v_{\rm ps} \; = \; v_{\rm eff}(\vec{r}) \; + \; \sum_i \left(\varepsilon_v \; - \; \varepsilon_{c_i}\right) |\psi_{c_i}\rangle \, \langle\psi_{c_i}| \; . \tag{77}$$

$v_{\rm ps}$ non-local and energy-dependent

$|\psi_{\rm ps}\rangle$ is not normalized

Norm-conserving pseudopotentials

Construction scheme

Asymptotically pseudopotential should describe the long-range interaction of the core

Outside of a core radius r_c the pseudo-wavefunction should coincide with the full wavefunction

Inside of this radius both the pseudopotential and the wavefunction should be as smooth as possible ($\rightarrow$ softness)

The requirement of norm conservation automatically ensures that it has the same one-particle energy ε_v as the true valence wave function

Example

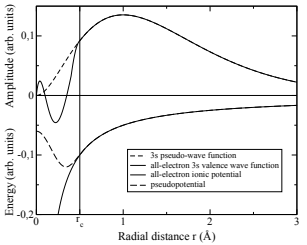

Schematic illustration of the difference between the all-electron (solid line) and pseudo $3s$ wave function (dashed line) and their corresponding potentials. The core radius r_c is indicated by the vertical line.

Ultrasoft Pseudopotentials

Norm-conserving constraint removed

Constructed by a generalized orthonormality condition

In order to recover the correct charge density, augmentation charges are introduced in the core region

The electron density subdivided in a delocalized smooth part and a localized hard part in the core regions

$\Rightarrow$ Dramatic reduction in the neccessary size of a plane-wave basis set

Plane wave codes

DFT calculations first successfully applied to solid-state problems:
lattice constants, cohesive energies, bulk modulus, . . .

Natural basis for periodic structures: plane waves

$$\psi_{\rm i}^{\vec{G}}(\vec{r}) \; = \; \frac{1}{\sqrt{V}} \, e^{i(\vec{k}_{\rm i}+\vec{G})\cdot\vec{r}} \tag{78}$$

$\vec{G}$ reciprocal lattice vector

Plane waves are already of the form required by the Bloch theorem

Only plane waves that differ by a reciprocal lattice vector do couple:

$$\langle\psi_{\vec{k}}|h|\psi_{\vec{k}'}\rangle \; = \; 0 \qquad \text{for} \;\; \vec{k} \neq \vec{k}' + \vec{G} \; . \tag{79}$$

Plane wave codes II

For periodic, infinite systems, the band structure energy in the total energy expression has to be replaced by an integral over the first Brillouin zone:

$$\sum_i \varepsilon_i \longrightarrow \sum_{\text{bands}} \frac{V}{(2\pi)^3} \int_{BZ} d\vec{k}\ \varepsilon(\vec{k}) \tag{80}$$

Integral can be approximated rather accurately by a sum over a finite set of $\vec{k}$-points, either by using equally spaced $\vec{k}$-points or so-called *special $\vec{k}$-points*

Parameter characterizing the size of the plane wave basis: cutoff energy

$$E_{\text{cutoff}} = \max_{\vec{G}} \frac{\hbar^2(\vec{k}+\vec{G})^2}{2m} \tag{81}$$

Norm-conserving Troullier-Martins pseudopotentials:
cutoff energy ∼10 Ryd for semiconductors and ≥50 Ry for transition metals

Ultrasoft pseudopotentials: cutoff energy for transition metals reduced to about 20 Ryd ≈ 250 eV.

Plane wave codes for surface problems

Plane wave basis

Expansion of wave functions in plane waves computationally very efficient

Requires three-dimensional periodicity

Surfaces modelled in the super cell approach

Convergence checks:
Slab and vacuum thickness

Typical values:
slab at least four layers thick
vacuum layer ≥ 10 Å

Super cell

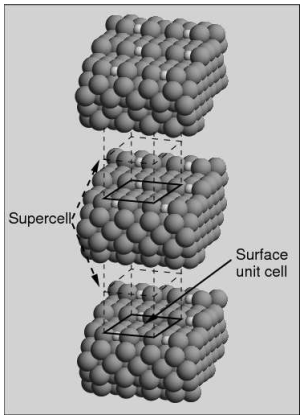

Augmented plane waves

Electronic structure method for extended systems that take into account the core electrons:

Main idea: Different basis set for core and for interstitial region.

First implementation: *muffin-tin potential*

$$v_{\text{eff}}(\vec{r}) = \begin{cases} 0 & \text{interstitial region} \\ v_{\text{MT}}(|\vec{r}-\vec{R}_i|) & |\vec{r}-\vec{R}_i| < r_{\text{MT}} \end{cases}, \tag{82}$$

Basis set: *Augmented plane waves* (APW)

$$\phi_{\vec{k},\varepsilon}(\vec{r}) = \begin{cases} \frac{1}{\sqrt{V}}\, e^{i\vec{k}\cdot\vec{r}} & \text{interstitial region} \\ \sum_{lm} a_{lm}(\vec{k},\varepsilon)\ u_l(r_i,\varepsilon)\ Y_{lm}(\theta,\phi) & r_i = |\vec{r}-\vec{R}_i| < r_{\text{MT}} \end{cases}, \tag{83}$$

Augmented plane waves II

$$\phi_{\vec{k},\varepsilon}(\vec{r}) = \begin{cases} \frac{1}{\sqrt{V}}\, e^{i\vec{k}\cdot\vec{r}} & \text{interstitial region} \\ \sum_{lm} a_{lm}(\vec{k},\varepsilon)\ u_l(r_i,\varepsilon)\ Y_{lm}(\theta,\phi) & r_i = |\vec{r}-\vec{R}_i| < r_{\text{MT}} \end{cases}, \tag{84}$$

$u_l(r,\varepsilon)$ solutions of the radial Schrödinger equation

$$\left\{ -\frac{\hbar^2}{2m}\frac{d^2}{dr^2} + \frac{\hbar^2}{2m}\frac{l(l+1)}{r^2} + v_{\text{MT}}(r) - \varepsilon \right\} r u_l(r,\varepsilon) = 0\,. \tag{85}$$

Important: there is no constraint relating $\vec{k}$ and ε

Correct solution expanded as

$$\psi_{\vec{k}}(\vec{r}) = \sum_{\vec{G}} c_{\vec{G}}\ \phi_{\vec{k}+\vec{G},\varepsilon}(\vec{r})\,, \tag{86}$$

Problem: basis functions depend on energy ε

Linearized augmented plane waves

Problem of energy-depended basis functions avoided by the concept of linearized augmented plane waves (LAPW): O.K. Andersen (1975)

Idea: expand radial function around fixed energy ε_l:

$$u_l(r,\varepsilon) \;=\; u_l(r,\varepsilon_l) \;+\; \dot{u}_l(r,\varepsilon_l)\,(\varepsilon-\varepsilon_l) \;+\; \ldots\;, \tag{87}$$

$\dot{u}_l(r,\varepsilon_l)$ energy derivative

$$\dot{u}_l(r,\varepsilon_l) \;=\; \left.\frac{du_l(r,\varepsilon)}{d\varepsilon}\right|_{\varepsilon=\varepsilon_l}\;. \tag{88}$$

ε_l should be in the middle of the corresponding energy band with l character.

Linearized augmented plane waves II

LAPW basis functions:

$$\phi_{\vec{k}}(\vec{r}) \;=\; \begin{cases} \frac{1}{\sqrt{V}}\,e^{i\vec{k}\cdot\vec{r}} & \text{interstitial region} \\ \sum\limits_{lm}\Big[a_{lm}(\vec{k})\;u_l(r_i,\varepsilon_l) \;+ \\ \quad b_{lm}(\vec{k})\;\dot{u}_l(r_i,\varepsilon_l)\Big]\;Y_{lm}(\theta,\phi) & |\vec{r}-\vec{R}_i|<r_{\mathrm{MT}} \end{cases} \tag{89}$$

$a_{lm}(\vec{k})$ and $b_{lm}(\vec{k})$ determined through the continuity requirement of both the wave function and its first derivative.

FP-LAPW: no restriction to spherical symmetric potentials in the core region

$$v_{\mathrm{eff}}(\vec{r}) \;=\; \begin{cases} \sum\limits_{\vec{G}}\;v_{\mathrm{eff}}(\vec{G})\;e^{i\vec{G}\cdot\vec{r}} & \text{interstitial region} \\ \sum\limits_{lm}v^{lm}_{\mathrm{eff}}(r_i)\;Y_{lm}(\theta,\phi) & |\vec{r}-\vec{R}_i|<r_{\mathrm{MT}} \end{cases}\;. \tag{90}$$

Tight-Binding

Ab initio electronic structure methods still computationally expensive

There is a need for a approximative method that retains the quantum nature of bonding: Tight-binding

Tight-binding: expansion of the eigenstates of the effective one-particle Hamiltonian in an atomic-like basis set and replacing the exact many-body Hamiltonian with parametrized Hamiltonian matrix elements

Formally, one starts with a basis of atomic functions

$$\phi_{i\alpha}(\vec{r}) \;=\; \phi_\alpha(\vec{r}\;-\;\vec{R}_i)\;, \tag{91}$$

i lattice site, α type of the atomic orbital

Periodic functions constructed by forming Bloch sums

$$\phi_{\alpha\vec{k}}(\vec{r}) \;=\; \frac{1}{\sqrt{N}}\sum_i\;e^{i\vec{k}\cdot\vec{R}_i}\;\phi_\alpha(\vec{r}\;-\;\vec{R}_i)\;, \tag{92}$$

Tight-Binding II

Bloch sums are used to determine Hamiltonian matrix elements:

$$\begin{aligned} h_{\alpha\beta}(\vec{k}) \;&=\; \langle\phi_{\alpha\vec{k}}|h|\phi_{\beta\vec{k}}\rangle \\ &=\; \sum_j\;e^{i\vec{k}\cdot\vec{R}_j}\;\langle\phi_{0\alpha}|h|\phi_{j\beta}\rangle \;=\; \sum_j\;e^{i\vec{k}\cdot\vec{R}_j}\;h_{\alpha\beta}(\vec{R}_j)\;. \end{aligned} \tag{93}$$

Two-center approximation for $h_{\alpha\beta}(\vec{R}_j)$:

$h_{\alpha\beta}(\vec{R})$ function of $R=|\vec{R}|$ and of the direction cosines k,l,m of $\vec{R}$.

Eigenfunctions $\chi_{\vec{k}}$ of the one-particle Hamiltonian

$$\chi_{\vec{k}}(\vec{r}) \;=\; \sum_\alpha\;c_\alpha(\vec{k})\;\phi_{\alpha\vec{k}}(\vec{r})\;. \tag{94}$$

Nonorthogonal tight-binding

Eigenfunctions $\chi_{\vec{k}}$ of the one-particle Hamiltonian

$$\chi_{\vec{k}}(\vec{r}) \;=\; \sum_{\alpha} \; c_{\alpha}(\vec{k}) \; \phi_{\alpha\vec{k}}(\vec{r}) \; . \tag{95}$$

Energies determined by eigenvalue equation

$$h(\vec{k}) \; c(\vec{k}) \;=\; S(\vec{k}) \; \varepsilon(\vec{k}) \; c(\vec{k}), \tag{96}$$

$S(\vec{k})$ overlap matrix

$$S_{\alpha\beta}(\vec{k}) \;=\; \sum_{j} \; e^{i\vec{k}\cdot\vec{R}_j} \; \langle\phi_{0\alpha}|\phi_{j\beta}\rangle \;=\; \sum_{j} \; e^{i\vec{k}\cdot\vec{R}_j} \; S_{\alpha\beta}(\vec{R}_j) \; . \tag{97}$$

$\Rightarrow$ Dispersion curves $\varepsilon(\vec{k})$ obtained by the diagonalization of $S(\vec{k})^{-1}h(\vec{k})$.
Nonorthogonal tight-binding

Orthogonal tight-binding

Further simplification: Assume that the atomic orbitals are already orthogonalized according to the Löwdin scheme

$$\psi_{i\alpha}(\vec{r}) \;=\; \sum_{j\beta} \; S^{-1/2}_{i\alpha j\beta} \; \phi_{j\beta}(\vec{r}) \; , \tag{98}$$

$\Rightarrow$ Dispersion curves $\varepsilon(\vec{k})$ obtained by the diagonalization of $h(\vec{k})$.

N_c atoms in the unit cell and l atomic orbitals per atoms
$\Rightarrow N_c l \times N_c l$ matrix has to be diagonalized

Atomic basis function do not explicitly appear in tight-binding
$\Rightarrow$ parametrization scheme determines the reliability and accuracy of any tight-binding calculation

Total energies in tight-binding

Total energies: usually a repulsive term written as a sum of pair terms is added to the band energy (can be derived from DFT)

$$\begin{aligned} E_{\rm tot} \;&=\; E_{\rm band} \;+\; E_{\rm rep} \\ &=\; \sum_{\vec{k}} \varepsilon(\vec{k}) \;+\; \sum_{ij} U_{ij} \; . \end{aligned} \tag{99}$$

Tight-binding useful scheme to understand qualitative trends.
Example: dispersion for a s-band in a metal under the assumption of only nearest neighbors (nn) interaction

$$\varepsilon(\vec{k}) \;=\; \beta \;+\; \sum_{nn} \gamma \; \cos\vec{k}\cdot\vec{R} \; , \tag{100}$$

$\beta = \langle\phi_{0s}|h|\phi_{0s}\rangle$ *on-site* term, $\gamma = \langle\phi_{0s}|h|\phi_{(nn)s}\rangle$

fcc crystal: s-band width $= 12\gamma$ $\quad\rightarrow$ proportional to overlap integrals

Structure and energetics of clean surfaces

Surface energies

Surfaces can be assumed to be created by cleaving an infinite solid

This requires energies, otherwise crystal would cleave spontaneously

Calculated surface energies of a monoatomic solid at 0K:

$$\gamma \;=\; \frac{1}{2A} \; (E_{\rm slab} - N \cdot E_{\rm bulk}) \tag{101}$$

$E_{\rm slab}$ total energy of the slab per supercell,
$E_{\rm bulk}$ is the bulk cohesive energy per atom,
A is the surface area in the supercell.

Experiment

Experimental determination of surface energies non-trivial

Usually surface energies are not directly measured, but only relative to other surfaces

Many reported surface energies are derived from surface tension measurements in the liquid phase and extrapolated to zero temperature

$\Rightarrow$ These surface energies correspond to an average over different orientations

Electronic states of surfaces and adsorbates

Ground state energy in density functional theory:

$$E = \sum_{i=1}^{N} \varepsilon_i + E_{\rm xc}[n] - \int v_{\rm xc}(\vec{r}) n(\vec{r})\, d^3\vec{r} - V_{\rm H} + V_{\rm nucl-nucl} \qquad (102)$$

Energy contributions

Band structure term:

$$E_{\rm bs} = \sum_{i=1}^{N} \varepsilon_i \qquad (103)$$

Exchange-correlation energy:

$$E_{\rm xc}[n] - \int v_{\rm xc}(\vec{r}) n(\vec{r})\, d^3\vec{r} \qquad (104)$$

Hartree energy:

$$V_{\rm H} = \frac{1}{2} \int \frac{e^2 n(\vec{r}) n(\vec{r}')}{|\vec{r} - \vec{r}'|}\, d^3\vec{r} d^3\vec{r}' \,. \qquad (105)$$

Electostatic nucleus-nucleus interaction:

$$V_{\rm nucl-nucl} = \frac{1}{2} \sum_{\rm I \neq J} \frac{Z_{\rm I} Z_{\rm J} e^2}{|\vec{R}_{\rm I} - \vec{R}_{\rm J}|} \,. \qquad (106)$$

Discussion

- Recall that fundamental Hamiltonian only contains kinetic and electrostatic energy
- Exchange-correlation and Hartree energy also included in the Kohn-Sham eigenvalues ε_i (double counting)
- Correction $E_{\rm xc}[n] - \int v_{\rm xc}(\vec{r}) n(\vec{r}) d^3\vec{r} - V_{\rm H}$ reflects the interaction of the particles
- The following discussion will mainly focus on the band structure term

Density of states

Local density of states (LDOS) useful tool to discuss the reactivity of surfaces

$$n(\vec{r}, \varepsilon) = \sum_i |\phi_i(\vec{r})|^2\, \delta(\varepsilon - \varepsilon_i) \qquad (107)$$

Derived quantities

⇒ Total density of states:

$$n(\varepsilon) = \int n(\vec{r}, \varepsilon)\, d^3\vec{r} \qquad (108)$$

⇒ Total Electron density:

$$n(\vec{r}) = \int n(\vec{r}, \varepsilon)\, d\varepsilon \qquad (109)$$

⇒ Band structure term:

$$\sum_{i=1}^{N} \varepsilon_i = \int n(\varepsilon)\, \varepsilon\, d\varepsilon \qquad (110)$$

Projected density of states:

$$n_a(\varepsilon) = \sum_i |\langle \phi_i | \phi_a \rangle|^2\, \delta(\varepsilon - \varepsilon_i) \qquad (111)$$

Example

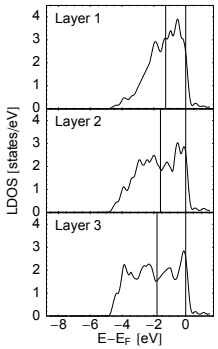

d-LDOS of the three top Pd(210) layers (M. Lischka and A. Groß, Phys. Rev. B 65, 075420 (2002))

Jellium model

Model description

Positive ion charges replaced by a uniform charge background:

$$n_+(\vec{r}) = \begin{cases} \bar{n}, & z \leq 0 \\ 0, & z > 0 \end{cases} \,. \qquad (112)$$

Electrons spill out into the vacuum
⇒ Dipole layer

Screening of the positive background by the electrons incomplete since only electrons with wave vectors up to the Fermi wave vector k_F are available

⇒ Friedel oscillations with wavelength π/k_F

Charge density

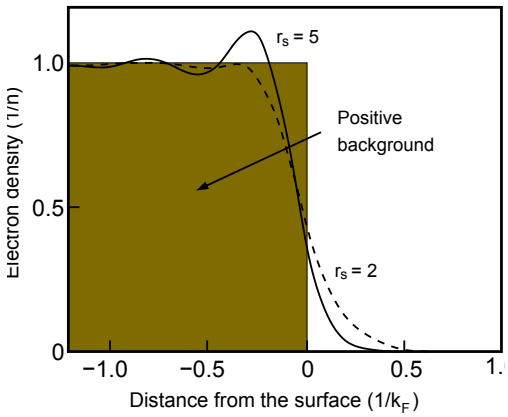

Charge density at a surface in the jellium model

Work function

Definition

Work function Φ: minimum energy that must be done to remove an electron from a solid at 0K.

$$\begin{aligned} \Phi &= \phi(\infty) + E_{N-1} - E_N \\ \Phi &= \Delta\phi - \bar{\mu} \\ &= \phi(\infty) - \varepsilon_F \,, \end{aligned} \qquad (113)$$

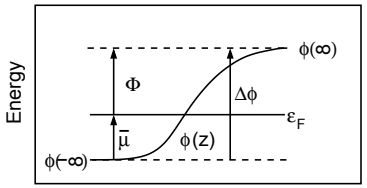

Jellium results

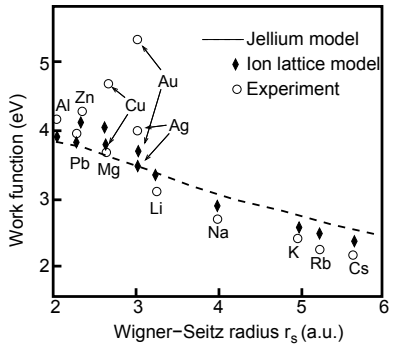

Jellium model surprisingly good for the description of simple sp-bonded metals, but fails for d-metals such as Au, Ag, Cu, ...

⇒ Realistic surface structure has to be taken into account

Electronic band structure at surfaces

At surfaces,symmetry broken in z-direction

$\Rightarrow$ k_z no longer a good quantum number

Projected bulk band structure

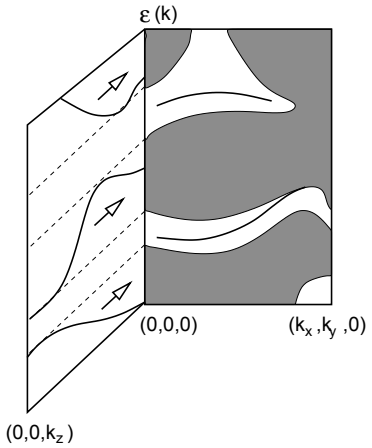

Discussion

Electronic band structure along k_z projected onto $k_x k_y$-plane

In gaps, localized surface states can exist: *Shockley surface states*, whose existence can be derived within the one-dimensional nearly-free electron model:

$$V(z) = V_0 + W_0\Theta(-z) + V_G\cos(Gz)\,\Theta(z)\,.$$

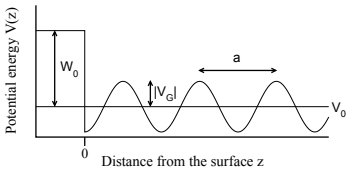

Surface states that join the bulk continuum: Surface resonances

Electronic surface states

DFT surface band structure of Cu(111)

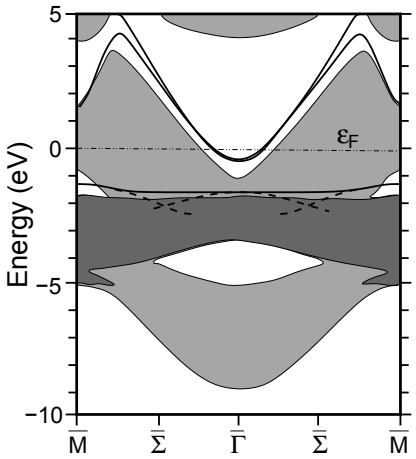

A. Euceda, D.M. Bylander, and L. Kleinman, Phys. Rev. B **28**, 528 (1983)

Discussion

Cu(111): Bandgap and parabolic surface band at the $\bar{\Gamma}$ point

Effective mass: $m^* = 0.37 \cdot m_e$ corresponds to Shockley state in the sp-band gap

Surface state 1.5 eV below Fermi level: Tamm surface state that is pushed out of the d band

Caused by the strong perturbation of the local atomic orbitals

True surface state since it is orthogonal to the sp-continuum

Surface resonances emanating from the Tamm surface band

Tamm surface states in tight-binding

Consider an equidistant linear chain of identical atoms having only one s orbital $|\phi_l\rangle$ at each site l. Use the orthogonal tight-binding approximation with only nearest-neighbor interactions. The on-site and hopping matrix elements are given by

$$\langle\phi_l|h|\phi_m\rangle = \beta\delta_{l,m} + \gamma\delta_{l,m\pm1}\,. \qquad (114)$$

"Bulk" band structure can be determined for an infinite chain of atoms.

Consider a semi-infinite chain of atoms with sites $n = 0, 1, \ldots$ as a model for a crystal with a surface. The on-site term for the surface atom differs from the bulk value, i.e.

$$\langle\phi_0|h|\phi_0\rangle = \beta' \neq \beta\,. \qquad (115)$$

For a strong perturbation of the on-site term at the surface $|\beta' - \beta| > |\gamma|$, new states above and below the bulk continuum appear, the so-called *Tamm surface states*, which are localized at the surface.

Cu(111) surface states

Don Eigler, IBM Almaden

Quantum Corral

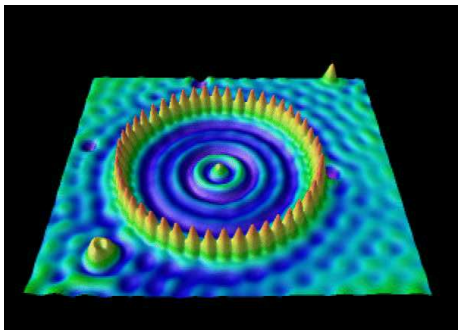

Standing surface waves

48 Fe atoms deposited on Cu(111) in a circle of diameter 71 Å

M.F. Crommie *et al.*, Science **262**, 218 (1993).

Quantum Mirage

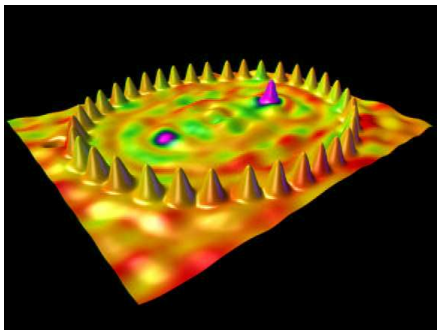

Kondo resonance effect

Elliptical *Quantum Corral* with a Co atom in the focal point of the ellipse

H.C. Manoharan *et al.*, Nature **403**, 512 (2000).

Image potential states on Cu(100)

Charge density of Cu(100)

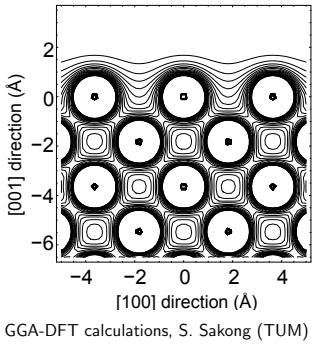

GGA-DFT calculations, S. Sakong (TUM)

Cu(100): surface band structure similar to Cu(111), but band gap at the $\bar{\Gamma}$ point extends above the vacuum level

Electrons with small parallel momentum can not penetrate into the bulk

⇒ Image potential states

Image potential

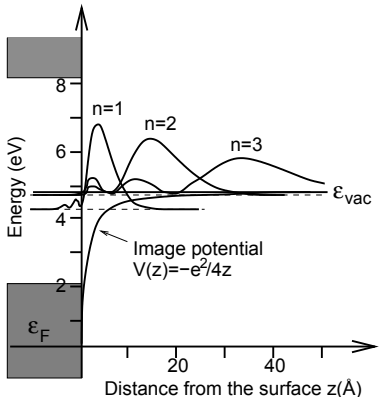

Rydberg-image potential states detected with time-resolved photoelectron spectroscopy

U. Höfer, I.L. Shumay, Ch. Reuß, U. Thomann, W. Wallauer, and Th. Fauster, Science **277**, 1480 (1997)

Trends in the energetics and structure of Cu surfaces

Surface energies

The more densely packed a certain lattice plane, the less bonds have to be broken upon cleavage.

Low-index surfaces:
$\gamma_{(111)} < \gamma_{(100)} < \gamma_{(110)}$

$((2n-1),1,1)$ surfaces: in fact $n(100)\times(111)$ surfaces

Large n: $\gamma_{((2n-1),1,1)} \rightarrow \gamma_{(100)}$
⇒ surf. energy decreases with increasing n.

From the sequence of $((2n-1),1,1)$ surface energies the step formation energy can be derived.

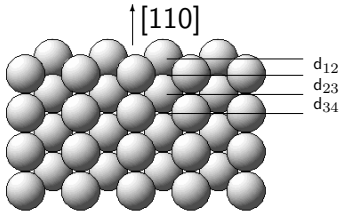

At metal surfaces, the smoothening of the electron density usually leads to a contractive relaxation of the first layer.

Inward relaxation causes a charge accumulation at the second layer ⇒ expansion

Smoluchowski smoothing of the electron density

Cu(100) surface

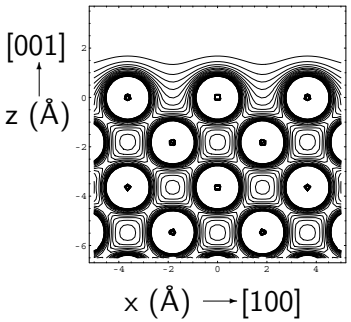

Schematic illustration

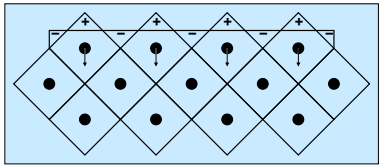

Wigner-Seitz (WS) cells at the (100) surface of a fcc crystal

Kinetic energy of electrons at the surface reduced by the smoothing

Qualitative picture of first-layer relaxation of metal surfaces

Electron smoothing

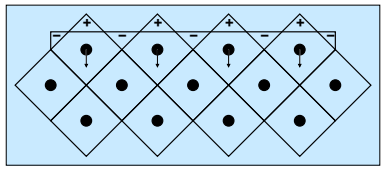

Wigner-Seitz (WS) cells at the (100) surface of a fcc crystal

Smoluchowski smoothing of electron density

Explanation

Assumption: $n(\vec{r})$ constant in the metal

Driving force: positively charge atomic core rearranges so that the electric field

$$\vec{E}(\vec{r}) = \int d\vec{r}'\; n(\vec{r}')\,\frac{(\vec{r}-\vec{r}')}{|\vec{r}-\vec{r}'|^3} \qquad (116)$$

outside of the WS cells is small

⇒ atomic core will be at the site where the electric field of the electron charge distribution vanishes, i.e. where

$$\int_{WS} d\vec{r}\; n(\vec{r})\,\frac{\vec{r}}{r^3} = 0 \qquad (117)$$

⇒ inward relaxation: (111) -1.6%, (100) -4.6%, (110) -16%

Surface energies and relaxations of Cu surfaces

Surface	Method	γ (J/m^2)	Δd_{12}	Δd_{23}	Δd_{34}	d_0(hkl) (Å)
Cu(111)	Theory	1.30	-0.9	-0.3		2.10
Cu(111)	Exp.	∼1.79	-0.7			2.08
Cu(100)	Theory	1.45	-2.6	1.5		1.821
Cu(100)	Exp.	∼1.79	-2.1	0.4	0.1	1.807
Cu(110)	Theory	1.53	-10.8	5.3	0.1	1.29
Cu(110)	Exp.	∼1.79	-8.5	2.3		1.28
Cu(311)	Theory	1.82	-15.0	4.0	-0.6	1.10
Cu(311)	Exp.		-11.9	1.8		1.09
Cu(511)	Theory	1.68	-11.1	-16.4	8.4	0.70
Cu(511)	Exp.		-14.2	-5.2	5.2	0.69

Calculated surface energies of 4d surfaces

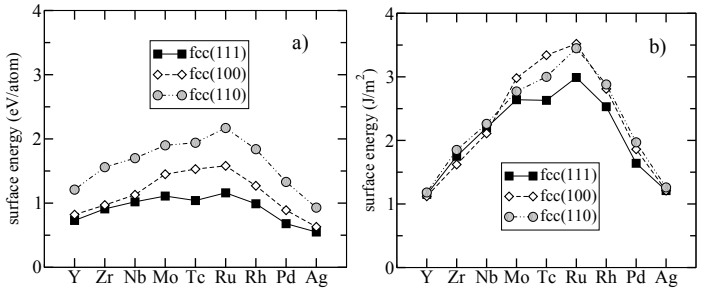

DFT-LDA surface energies for the 4d transition metals (Methfessel *et al.*, 1992)

Bond-cutting model: surface energy in tight-binding picture estimated by

$$\sigma = \frac{\sqrt{N_c^{bulk}} - \sqrt{N_c^{surf}}}{\sqrt{N_c^{bulk}}} E'_{coh} , \qquad (118)$$

N_c^{bulk} and N_c^{surf} coordination numbers, E'_{coh} cohesive energy

Semiconductor surfaces

Surface energies

Semiconductors are characterized by directional covalent bonds

Upon cleavage unsaturated highly unstable bonds, the *dangling bonds* are created

Surface tries to lower its energy by minimizing the number of dangling

Most prominent example: Si(111)-(7×7)

DAS model(Dimer-Adatom Stacking-fault): twelve top-layer adatoms, six rest atoms, a stacking fault in one of the two triangular subunits of the second layer, nine dimers and a deep corner hole

Si(111)-(7×7)

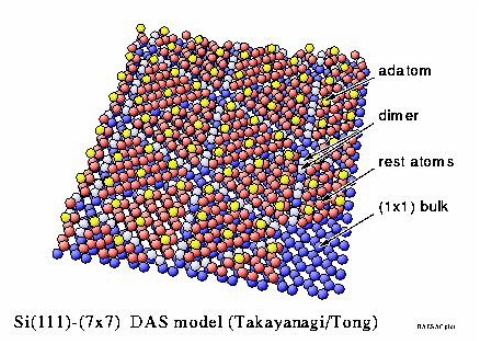

Si(111)-(7x7) DAS model (Takayanagi/Tong)

Semiconductor surfaces II

Surface electronic properties

Further driving force for reconstructions: semiconductor surfaces avoid to become metallic

Example: Si(100)-(2×2)

After dimerization still two half-filled dangling bonds at the Si(100)-(2×1) surface

The two half-filled dangling bond lead to a metallic surface state

⇒ Charge transfer: one dangling bond becomes completely filled, the other one empty, causing asymmetric buckled dimers

Mechanical surface stress released by alternating buckled dimers: (2×2) structure

Si(100)-(2×2)

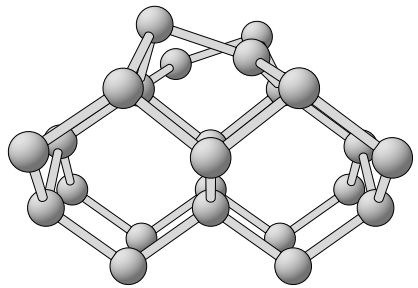

Si(100) (2×2) surface structure with alternating asymmetric buckled dimers.

Compound semiconductor surfaces

If the substrate consists of more than one element, then the surface energy depends on the specific thermodynamic conditions, i.e. the reservoir with which the atoms are exchanged in a structural transition.

Most stable surface structure determined by the minimum of the free energy.
Zero temperature:

$$\gamma = \frac{1}{A}\left(E_{\rm surf} - \sum_i \mu_i N_i\right) . \qquad (119)$$

Surface energy of GaAs: written as a function of a single variable such as, e.g., $\mu_{\rm As}$:

$$\gamma = \frac{1}{A}\left[E_{\rm surf} - \mu_{\rm GaAs}\, N_{\rm Ga} - \mu_{\rm As}\,(N_{\rm As} - N_{\rm Ga})\right] . \qquad (120)$$

GaAs(100)

GaAs(100) surface structures:

(a) (1×1) (b) α(2×4)

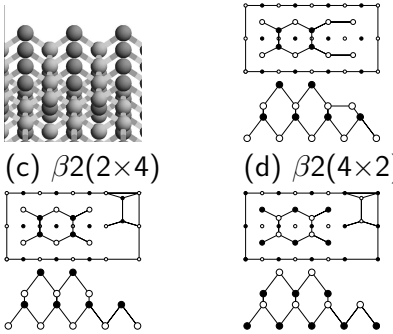

(c) β2(2×4) (d) β2(4×2)

Discussion

Filled circles: As atoms,
empty circles: Ga atoms

α(2×4) and β2(2×4): As-terminated,
β2(4×2): Ga-terminated

Ideal (1×1) structure highly unstable because of the dangling bonds

Electron-counting principle:

Anion dangling bonds filled and cation dangling bonds empty

⇒ Charge transfer from Ga to As
Filled p orbitals of As favor perpendicular bonds, sp^2-like hybridization of Ga favors planar configuration

GaAs(100): Stoichiometry

GaAs(100) surface structures:

(a) (1×1) (b) α(2×4)

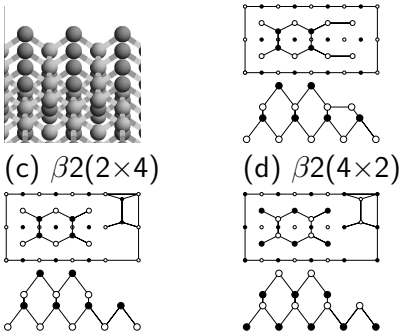

(c) β2(2×4) (d) β2(4×2)

Stoichiometry

Stoichiometry $\Delta N = N_{\rm As} - N_{\rm Ga}$:
(1×1) As-terminated surface $\Delta N = \frac{1}{2}$
(1×1) Ga-terminated surf. $\Delta N = -\frac{1}{2}$
Derivation → symmetric slab

α(2×4) structure: $\Delta N = 0$
β2(2×4): $\Delta N = \frac{1}{4}$ per 1×1 unit cell
β2(4×2): $\Delta N = -\frac{1}{4}$ per 1×1 unit cell

Stoichiometry and surface energies not obvious, if the slab has two inequivalent surfaces as, e.g., the (111) and $(\bar{1}\bar{1}\bar{1})$ surfaces of zinc-blende-structures

⇒ Energy density formulation (Chetty and Martin)

GaAs(100): Surface energies

GaAs(100) surface energies:

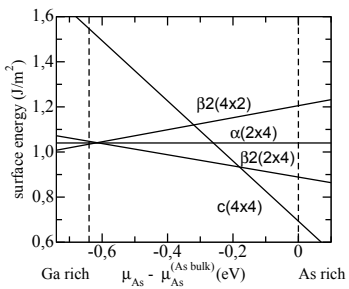

Surface energies of different GaAs(100) reconstructions in J/m^2 as a function of the difference of the chemical potential of As and bulk As (Moll *et al*, 1996).

Discussion

GaAs tries to minimize the number of dangling bonds by dimerization

Further driving force: electrostatics

β2 structures minimize the electrostatic repulsion

Planar Ga-terminated configuration energetically more costly than uotward relaxation of As-terminated structures

⇒ Ga-terminated β2(4×2) surface is only stable under extrem Ga rich conditions

Insulator surfaces

NaCl structure

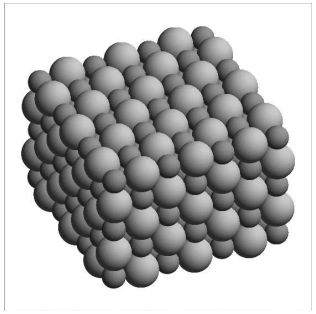

Sodium chloride structure

Ionic surfaces

NaCl structure: Two fcc sublattices translated by $a/2(\vec{e}_x + \vec{e}_y + \vec{e}_z)$

Electrostatic potential outside of a slab structure:

$$\phi(z \to \infty) = \phi_G \, e^{-\frac{2\pi}{z}a} \; + \; 2\pi\sigma_\perp \quad (121)$$

$\sigma_\perp$: dipole moment perpendicular to the plane per unit area

Polar surface highly unstable

Nonpolar surface: electrostatic potential falls off very rapidly, surface termination almost ideal

Polar ionic oxide surface: $Al_2O_3(0001)$

α-$Al_2O_3(0001)$ surface important substrate for very high frequency microelectronic devices due to its insulating character

$Al_2O_3(0001)$ surface structure:

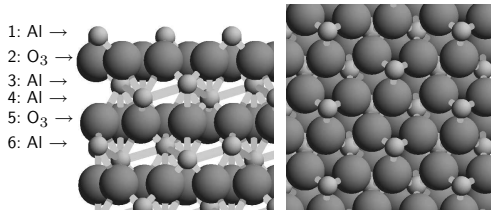

Side and top view of the Al-terminated α-$Al_2O_3(0001)$ surface.

Al_2O_3

α-Al_2O_3 (sapphire) cystallizes in the corundum structure

Rhombohedral unit cell: 2 Al_2O_3 formula units

Hexagonal unit cell: 12 Al atoms and 18 O atoms
O atoms stacked in slightly distorted hcp structure
Al atoms occupy 2/3 of octahedral holes in O sublattice

$Al_2O_3(0001)$: Surface energies

$Al_2O_3(0001)$ surface energies:

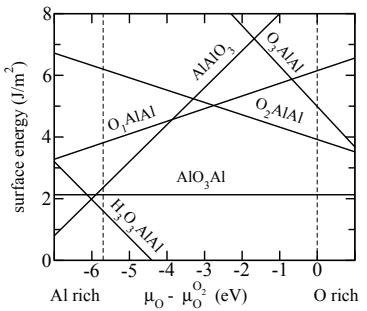

Surface energies of different $Al_2O_3(0001)$ (1×1) structure in J/m^2 as a function of the difference of the oxygen chemical potential (Wang *et al* (2000), Batyrev *et al.* (1999)).

Discussion

(1×1) structures stable, no reconstructions

Stoichiometric AlO_3Al-termination stable over the entire range of oxygen chemical potentials

Non-stoichiometric surfaces metallic

Oxygen-terminated surface only by hydrogenation stable

$Al_2O_3(0001)$ surface relaxations

Interlayer-		Theory[a] GGA	Theory[b] LDA	Theory[c] LDA	Theory[d] LDA	Exp.[e]	Exp.[f]
Al-O_3	1-2	-86	-87	-85	-77	-51	+30
O_3-Al	2-3	+6	+3	+3	+11	+16	+6
Al-Al	3-4	-49	-42	-45	-34	-29	-55
Al-O_3	4-5	+22	+19	+20	+19	+20	–
O_3-Al	5-6	+6	+6	–	+1	–	–

[a] Wang *et al.*(GGA), [b] Verdozzi *et al.*(LDA), [c] Di Felice *et al.*(LDA), [e] Guenard *et al.*, [d] Batyrev *et al.*, [f] Toofan *et al.*.

Significant first-layer contraction in order to minimize surface dipole

Exp. f) Probably hydrogenated O-terminated surface

$Al_2O_3(0001)$ surface reconstructions at higher temperatures

Above $T = 1350$ K, oxygen evaporates from the top layers

⇒ Complex Al-rich structures addressed with empirical potentials
hexagonal and square arrangement of Al atoms in top layer

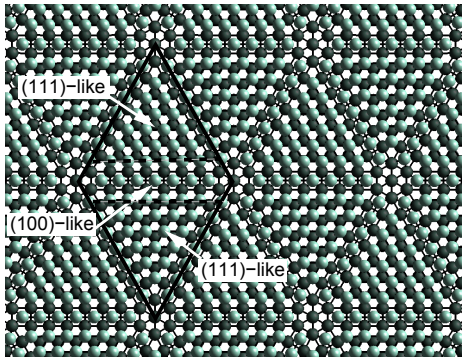

$(3\sqrt{3} \times 3\sqrt{3})$r30° reconstructed α-$Al_2O_3(0001)$ surface obtained by simulations using empirical potentials
I. Vilfan *et al.*, Surf. Sci. **505**, L215 (2002)

Ultrathin $Al_2O_3(0001)$ films on NiAl(110)

STM: conducting substrate needed

⇒ Deposite ultrathin oxide films on metal substrate → $Al_{10}O_{13}$ film

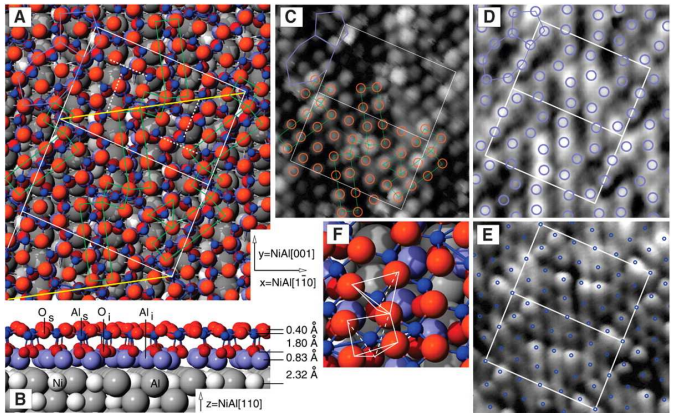

Structure of ultrathin Al_2O_3 on NiAl(110): STM and DFT calculations
G. Kresse *et al.*, Science **308**, 1440 (2005)

Strong Ni-Al interaction plus hexagonal and square Al arrangement in top layer

Scanning tunneling microscope (STM)

Principle

Animation

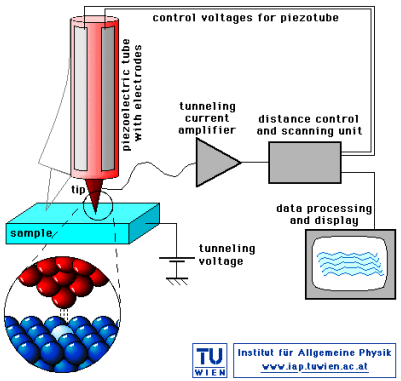

Michael Schmid, TU Wien

Michael Schmid, TU Wien

Interpretation of STM pictures

Graphite(0001)

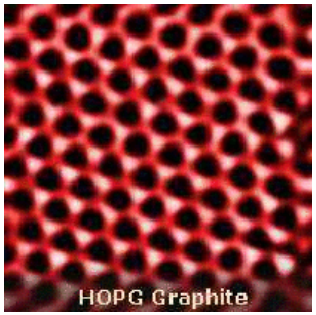

HOPG: Highly Oriented Purified Graphite

Discussion

STM constant height modus:
Magnitude of tunneling current is monitored

⇒ Atoms are not directly imaged, but current distribution

Graphite: Honeycomb net not reproduced in STM pictures, every second atom is missing

⇒ Electronic structure calculations are needed in order to understand STM pictures

Tersoff-Hamann picture

Tunneling current

$$I = \frac{2\pi e}{\hbar} \sum_{\mu\nu} f(E_\mu)[1 - f(E_\nu)] \times |M_{\mu\nu}|^2 \delta(E_\mu - (E_\nu + eV)) \quad (122)$$

Tersoff-Hamann ($\vec{r}_t$; tip position):

$$I \propto \sum_{\nu} |\psi(\vec{r}_t)|^2 \delta(E_\mu - E_\nu) = \rho(\vec{r}_t, E_F) \quad (123)$$

Simulated STM picture

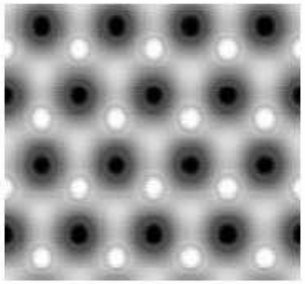

Graphite(0001) (Courtesy of T. Markert)

Perturbation approach

Also known as Bardeen approach (Bardeen, 1961)

Tunneling current

Sample and tip treated as separate entities

$$I = \frac{4\pi e}{\hbar} \sum_{\mu\nu} \left| \int_S \left(\chi_\mu^* \nabla\psi_\nu - \psi_\nu \nabla\chi_\mu^*\right) \right|^2 \times \delta(E_\mu - (E_\nu + eV)) \quad (124)$$

χ_μ: eigenstates of the STM tip
ψ_ν: eigenstates of the surface
S: separation surface between tip and surface

Simulated STM picture

Maleic anhydride ($C_4H_2O_3$) on Si(100)

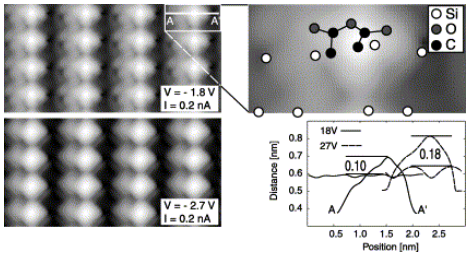

W. Hofer *et al.*, Chem. Phys. Lett. **355**, 3437 (2002).

⇒ Tunneling current proportional to overlap of wave functions

Simulation necessary for interpretation of STM picture